Check for updates

Stabilizing LiNi$_{0.8}$Co$_{0.15}$Mn$_{0.05}$O$_2$ Cathode by Doping Sulfate for Lithium-Ion Batteries

Jianying Li,[a] Jian Wu,[a] Shaomin Li,[a] Guobiao Liu,[a] Yanhua Cui,[b] Zhaohui Dong,*[c] Hao Liu,*[a] and Xueliang Sun[d]

Residual sulfate (SO$_4^{2-}$) in precursor Ni$_{0.8}$Co$_{0.15}$Mn$_{0.05}$(OH)$_2$ (pre-NCM) is commonly regarded as being harmful to Li-[Ni$_{0.8}$Co$_{0.15}$Mn$_{0.05}$]O$_2$ (NCM) performance, leading to significant performance losses and also hampering the electrode fabrication. Therefore, manufacturers try their best to lower sulfate contents in pre-NCM. However, how the sulfate affects the cathode materials is not systematically studied. To address these issues, NCM was synthesized with different amounts of intentionally added sulfate (NH$_4$)$_2$SO$_4$ in pre-NCM. It was demonstrated that anionic SO$_4^{2-}$ doped in NCM could influence the grain size in sintering process and stabilize the layer structure during the charge–discharge process at a certain doping amount. The first-principles calculations suggested that the SO$_4^{2-}$ doped in the transition metal layer could effectively facilitate Li$^+$ diffusion in the lattice. SO$_4^{2-}$ doping could reduce the energy barrier for Li$^+$ migration and then suppress drastic contraction of the c axis during cycling. The phase transition of H2 to H3 caused by c axis contraction was suppressed and the cycling performance was enhanced. The capacity retention could reach 80.9 (0.2 C) and 80.4% (1 C) after 380 and 240 cycles in coin cells, respectively. These findings illustrate that a certain amount of sulfate could be beneficial to NCM cathodes.

Introduction

Lithium-ion batteries (LIBs) have aroused attention with high power density and excellent circulation performance. They have been widely used in electric vehicles (EV) and hybrid electric vehicles (HEV) to resolve environment impact of the fossil fuel usage.[1,2] However, LIBs for EV and HEV need cells with even longer life and more stability. The power and energy density as well as the cycle life of LIBs should be further improved. Attention has been focused on the exploration of advanced cathode materials. Ni-rich layered cathode materials have been explored as good candidates for high-performance LIBs in recent years due to high energy density and capacity, reliable safety, and low toxicity.[3,4] As a typical Ni-rich cathode, Li[Ni$_{0.8}$Co$_{0.15}$Mn$_{0.05}$]O$_2$ (NCM) is able to deliver capacities as high as 200 mAh g^{-1} at a cut-off voltage of 2.5–4.3 V.[5,6]

[a] J. Li, J. Wu, S. Li, Dr. G. Liu, Prof. H. Liu
   Chengdu Development Center of Science and Technology of CAEP
   Chengdu, Sichuan, 610207 (P. R. China)
   E-mail: mliuhao@gmail.com
[b] Prof. Y. Cui
   Institute of Electronic Engineering
   China Academy of Engineering Physics
   Mianyang, Sichuan, 621000 (P. R. China)
[c] Prof. Z. Dong
   Shanghai Synchrotron Radiation Facility
   Shanghai Advanced Research Institute
   Chinese Academy of Sciences
   Shanghai, 201204 (P. R. China)
   E-mail: dongzhaohui@zjlab.org.cn
[d] X. Sun
   Department of Mechanical and Materials Engineering
   University of Western Ontario
   London, Ontario, N6A 5B9 (Canada)

Sulfates, such as NiSO$_4$, CoSO$_4$, and MnSO$_4$, are widely used to synthesize NCM as raw materials. SO$_4^{2-}$ remainder in cathode is hence unavoidable. It is generally considered that SO$_4^{2-}$ impurities have deleterious effects on the property of LIBs because the impurities generated from SO$_4^{2-}$ and metal ions may affect the crystallization of layered hydroxide precursors. The industry standard YS/T 798-2012 formulated by China's non-ferrous metals industry for NCM defines SO$_4^{2-}$ as impurity whose content should be less than 0.5 wt%. Cathode manufacturers go to great lengths to lower sulfate contents in NCM. To remove the SO$_4^{2-}$, the pre-NCM precipitate is often thoroughly rinsed with sufficient deionized water. The stringent SO$_4^{2-}$ content specifications lead to increased manufacturing cost.

However, SO$_4^{2-}$ polyanion compounds not only allow fast ion conduction but could stabilize the operative redox potentials of transition metals,[7] so a proper amount of SO$_4^{2-}$ residue should have a positive effect on the cathode materials. Recently, Ban et al.[8] reported a synthesis of Li$_2$SO$_4$-coated lithium-rich manganese-based cathode materials. The electrochemical performance of the cathode material was improved in terms of initial cycle efficiency and rate performance due to the formation of Li$_2$SO$_4$ on the surface of the particles. As a coating material, Li$_2$SO$_4$ can facilitate Li$^+$ diffusion at the solid particle interface. The results suggest that the sulfate does not necessarily have a detrimental effect on cathode performance. In addition, the SO$_4^{2-}$ polyanions can react with lithium residues (such as Li$_2$O/LiOH) to help to reduce the pH value of the cathode and enhance the stability of the surface structure.[9,10]

As for the industry, the cathode unavoidably contains sulfate "contamination", and these sulfates would inevitably react with transition metals (TM) and lithium ions at high temperature in the subsequent lithiation process. Different from previous reported coating mechanisms, the sulfates and their products would "doped" within the cathode materials, and the

ChemSusChem

Full Papers

doi.org/10.1002/cssc.202100595

Chemistry Europe
European Chemical
Societies Publishing

presence of such polyanions, as well as the final products, such as Li_2SO_4, would obviously affect the behavior of the cathode. Hence, it is necessary to identify the impact of doped SO_4^{2-} in NCM cathodes.

Herein, ammonium sulfate [$(NH_4)_2SO_4$, AS] was intentionally added into the precursor of Ni-rich cathode, and the performance of layered Ni-rich with sulfate impurities was comprehensively studied to identify the influencing mechanism of the residual sulfate. The results show that a proper amount of sulfate does not necessarily negatively affect the NCM structure but can work as a structure stabilizer to improve the electrochemical performance of the NCM cathodes, while an excess of sulfate can be harmful to cathode electrochemical performance. Various experimental techniques, as well as first-principles calculations, were used to study the decomposition of AS, the concentration of S element in particles, and the oxidation state of TM, in order to gain insights into the reason why the addition of SO_4^{2-} could improve cathode performance. Briefly, an appropriate doping of polyanions SO_4^{2-} into the layer of NCM particles can effectively stabilize the layer structure and enhance the electrochemical stability of the NCM cathode. The enhanced electrochemical performance is illustrated by rate performance test and charge/discharge cycling.

Experimental Section

The Supporting Information contains the following: scanning electron microscopy (SEM) images, X-ray diffraction (XRD) patterns, Fourier-transform infrared (FTIR) spectra, energy-dispersive X-ray spectroscopy (EDS) line scan profile, transmission electron microscopy (TEM) and high-resolution (HR)TEM images, X-ray photoelectron spectroscopy (XPS) spectra, initial charge and discharge curves, rate and cycling performance, SEM images of the electrodes after cyling, cyclic voltammetry (CV) curves, D_{Li+} from galvanostatic intermittent titration technique (GITT) curves, side and top views of the optimized geometries, Tables for residual sulfur contents, full width at half-maximum (FWHM) peaks, crystal structural parameters, initial charge/discharge capacities and coulombic efficiency, cycling performances, inductively coupled plasma (ICP) measurement, impedance parameters.

Synthesis of materials

NCM cathode materials were synthesized via the combination of a chemical co-precipitation method to prepare pre-NCM powders, and a succedent sintering process with the addition of $LiOH \cdot H_2O$. Briefly, a 2 M solution of $NiSO_4 \cdot 6H_2O$ (675.62 g) and $CoSO_4 \cdot 7H_2O$ (135.47 g) was made with a molar ratio of 0.845:0.1585. The solution, together with NaOH (2 M) solution and $NH_3 \cdot H_2O$ chelating agent solution, was concurrently pumped into a batch reactor (5 L) under N_2 flow. During the co-precipitation process, $Ni_{0.845}Co_{0.1585}(OH)_2$ (NC, Figure S1, Supporting Information) was firstly co-precipitated. After that, a 2 M $MnSO_4 \cdot H_2O$ (27.16 g) solution was slowly pumped into the batch reactor under O_2 atmosphere with a flow rate of 0.1 L min^{-1}. To achieve the concentration gradient (CG) structure layered oxides, Mn hydroxides were slowly piled onto the NC particles and pre-NCM (molar ratio of Ni/Co/Mn = 0.80:0.15:0.05) was achieved. The Mn concentration decreases while the Ni and Co content increases complementarily from the surface to the center throughout the particle. The pre-NCM powders were then filtered, washed by distilled water, and dried at 120 °C for 12 h.

To simulate the residual sulfate in NCM, pre-NCM powders were dispersed in distilled water, then AS was added into this suspension with different weight ratio of 0.5, 0.8, 1.0, and 1.2 wt%. The mixture was transferred into the vacuum oven and dried at 85 °C for 12 h. SEM images of the NC and pre-NCM are shown in Figure. S1. The obtained pre-NCM powders were then mixed with $LiOH \cdot H_2O$ in a molar ratio of 1:1.05 in an agate mortar. The mixture was transferred into a tube furnace and preheated at 500 °C for 3 h, and then the temperature was raised to 780 °C for 8 h in oxygen atmosphere with a flow rate of 0.25 L min^{-1}. The resultant cathode materials were marked as NCM, NCMS-1, NCMS-2, NCMS-3, and NCMS-4, respectively, presenting the original and AS-doped samples with various sulfate contents.

Analytical procedure

SEM (S-4800 microscope) was used to analyze the surface morphology of the samples. Semi-quantitative EDS of the cathode particle was collected on a Gemini SEM 300 SEM. Powder XRD with CuK_α radiation ($\lambda = 0.1541$ nm) was carried out to characterize the crystal structural properties of samples on a X'Pert-Pro MPD. The residual sulfur content in the NCM was measured with a carbon–sulfur (CS) determinator (LECO CS344). FTIR spectroscopy was performed on a JASCO 400 FTIR spectroscope. The oxidation state of TM and S element on particles surface was examined by XPS (ESCALAB 250Xi) with monochromatic AlK_α radiation. X-ray absorption near edge structure (XANES) spectra of the Ni K-edge ($E_0 = 8300$ eV), Co K-edge ($E_0 = 7700$ eV), and Mn K-edge ($E_0 = 6520$ eV) were measured in 0.5 eV steps at beam line BL15 U1 of the Shanghai Synchrotron Radiation Facility (SSRF), China. The data were recorded in a fluorescence mode, and a pure Ni and Mn foil were measured as reference. The quantitative analyses of Ni, Co, and Mn were performed by ICP spectroscopy. All materials for ICP analysis were dissolved in 10 wt% HNO_3.

Electrochemical measurements

The electrochemical characterizations were performed using CR2032 coin-type cells. The cathode slurry was prepared by mixing NCM powders, super P, and poly(vinylidenefluoride) (mass rate of 8:1:1) in N-methylpyrrolidinone (NMP). The slurry was then coated on a thin aluminum foil and dried in a vacuum oven at 110 °C for 12 h to remove the NMP. The foil was cut into circular electrodes with a diameter of 16 mm. The mass of the active loadings on the circular electrodes were around 4 mg cm^{-2}. Li metal (and commercial graphite) and a Celgard 2400 were used as anode and separator, respectively. The electrolyte was 1 mol L^{-1} $LiPF_6$ dissolved in ethylene carbonate/diethyl carbonate (EC/DEC) electrolyte. The coin cells were assembled in an argon-filled glovebox. The rate and cycling performances were measured between 2.8 and 4.3 V (vs. Li/Li$^+$) on an Arbin BT2000 instrument. A PARSTAT 4000 electrochemical workstation was used to measure the CV within the voltage range from 2.5 to 5 V with scan rate of 0.1, 0.2, 0.5, 1, 2, and 5 mV s^{-1}. GITT analysis was also tested at a pulse of 0.1 C for 15 min and with a time interval of 15 min until reaching the cutoff voltage. The Princeton V3 was used to measure electrochemical impedance spectroscopy (EIS) of the cells with a frequency range from 10 mHz to 10 kHz with an AC voltage of 5 mV amplitude.

ChemSusChem

Full Papers
doi.org/10.1002/cssc.202100595

Chemistry Europe
European Chemical
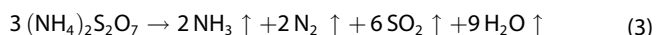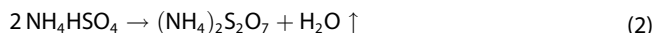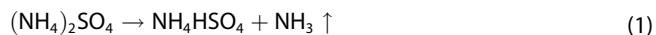Societies Publishing

First-principles calculations

The first-principles structure and energy calculations were performed with CP2 K/Quickstep package.[11] Goedecker–Teter–Hutter (GTH) pseudopotentials and double-ζ MOLOPT basis sets (DZVP-MOLOPT-SR-GTH) were used for all elements.[12,13] Perdew–Burke–Ernzerhof (PBE) electronic-correlation functional was used to describe the electronic structure.[14] In our calculation, the energy cutoff was set to 500 Ry. The convergence criterion for the geometry optimizations were set to 1.0×10^{-6} eV and 5.1×10^{-4} eV Å^{-1} for total energy and ionic force. The climbing image nudged elastic band (CI-NEB) method is used to optimize the Li-ion conduction pathways and the corresponding energy barriers.[15]

Initial configurations of NCM were constructed based on the $LiNiO_2$ (ICSD_78687.cif). Ni atoms in the oxygen octahedral are then replaced by Co and Mn atoms becoming a $LiNi_{1-x-y}Co_xMn_yO_2$ structure. Calculations were carried out on a $4 \times 4 \times 1$ supercell consisting of 192 atoms ($Li_{48}Ni_{40}Co_4Mn_4O_{96}$). Furthermore, the supercell was taken to build the configuration of $Li_{48}SNi_{39}Co_4Mn_4O_{96}$, in which S was constructed by replacing one Ni atom. All structural figures in this work were plotted using the VESTA software.[16]

Result and Discussion

The CS analysis was firstly carried out to verify the existence of sulfur in the cathode powders. The results listed in Table S1 show the sulfur content in the cathodes. As expected, the mass ratio of SO_4^{2-} increases from 0.21 to 0.82 wt% with the AS adding amount increasing from 0.5 to 1.2%. The weight loss is observed in the samples due to the decomposition of AS during sintering. $(NH_4)_2SO_4$ is converted to SO_2, NH_3, N_2, SO_2, and H_2O at around 270 °C according to the following side reactions.[17,18] The thermal decomposition stages can be represented by Equations (1)–(3):

$$(NH_4)_2SO_4 \rightarrow NH_4HSO_4 + NH_3 \uparrow \tag{1}$$

$$2\,NH_4HSO_4 \rightarrow (NH_4)_2S_2O_7 + H_2O \uparrow \tag{2}$$

$$3\,(NH_4)_2S_2O_7 \rightarrow 2\,NH_3 \uparrow +2\,N_2 \uparrow + 6\,SO_2 \uparrow +9\,H_2O \uparrow \tag{3}$$

The morphology of the materials was then characterized since they are of great importance to the battery performance.[19] The SEM images are shown in Figure 1a–e. NCMS has a slightly smaller grain size compared with the NCM sample. The FWHM was counted from XRD measurement to confirm this result. The second particle size of all samples is around 7–9 μm, as shown in Figure 1f and Figure S2.

The XRD patterns were indexed to a typical rhombohedral structure of a α-NaFeO$_2$ type (space group R-3m)[20,21] from Figure S3a. It is noteworthy that no clear peak of sulfate can be
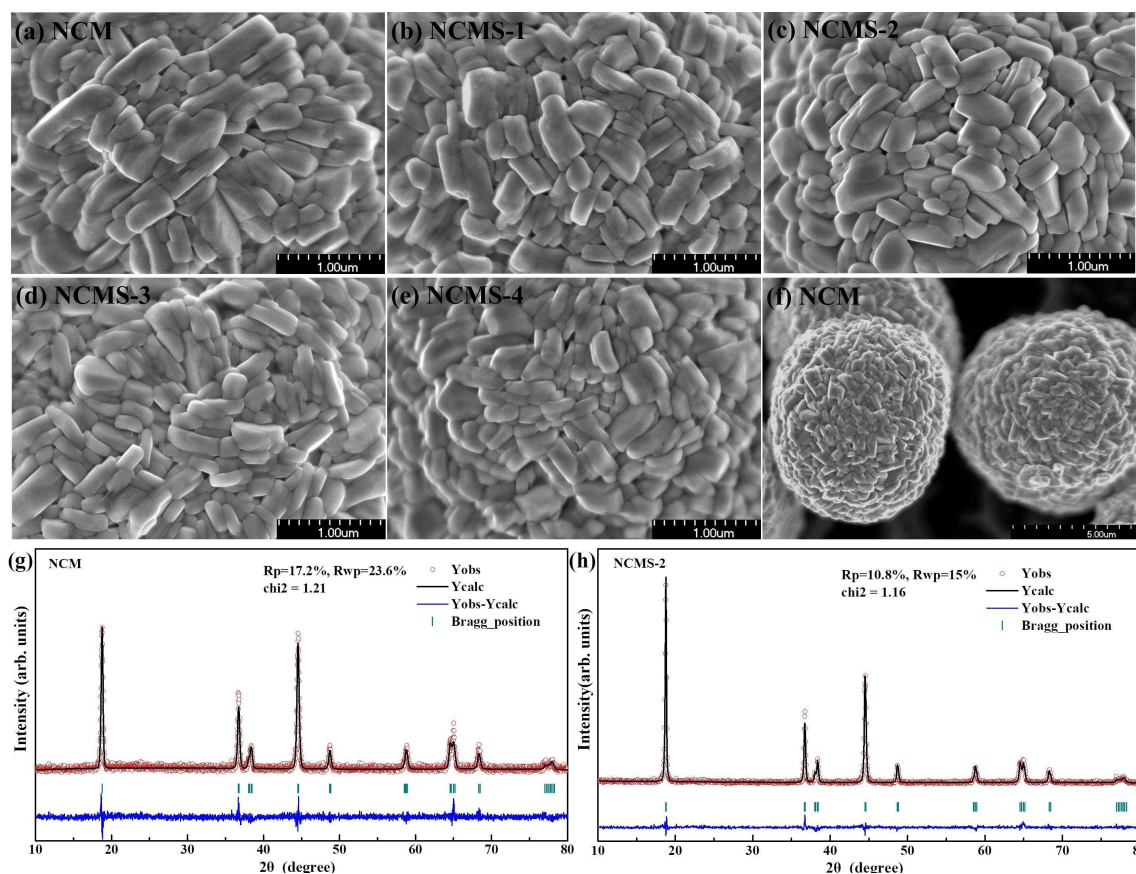

Figure 1. SEM images of (a) NCM, (b) NCMS-1, (c) NCMS-2, (d) NCMS-3, (e) NCMS-4. (f) Full view of the powder particles of NCM. Rietveld refinement of XRD patterns for (g) NCM and (h) NCMS-2.

ChemSusChem

Full Papers
doi.org/10.1002/cssc.202100595

Chemistry Europe
European Chemical
Societies Publishing

observed in the XRD patterns even at the highest SO_4^{2-} doping ratio (1.2 wt%). However, a distinct position shift toward lower angles can be observed on (003) and (104) diffraction peaks, owing to the incorporation of SO_4^{2-} as shown in Figure S3b,c. This shift can be attributed to the enlargement of fractional interlayer spacing in the [001] direction induced by the substitution of larger polyanions. Table S2 shows the FWHM of the (003) and (104) diffraction peak for the five samples. The FWHM of the sulfate doping cathode shows slightly upward trends. These trends are correlated with the decrease of grain size of the cathode because of the average size (plane of 003 and 104) is reflected by the inverse of the value of FWHM.[22,23] The results clearly evidence that the grain size is correlated with the anion doping of the cathode, because of the distortion of anion doping in the TM layer.[24] It should be noted that the anion intercalation is closely related to the cation mixing issues. The crystal structure of NCM and NCMS-2 was further analyzed by Rietveld refinement (Figure 1g,h). The corresponding analysis results (Table S3) indicate that the lattice parameter c is 14.169 Å in NCM, and it slightly increases in the modified sample. This phenomenon is consistent with the observation that $d(003)$ and $d(104)$ increase after sulfate doping. The modified sample has significantly reduced Li^+/Ni^{2+} cation mixing (1.55%) compared with NCM (2.57%). Therefore, the lower cation mixing degree in modified samples means that sulfate-doped structure can provide more ordered channel for fast Li^+ ions diffusion. In addition, a pillar effect may be caused by the polyanion doping in the lattice and further steady the layered structure during the long cycling.[25,26]

To determine the surface chemical composition, FTIR spectroscopy within the wave number from 400–4000 cm^{-1} was carried out on NCM samples (Figure S4). Compared with the pure NCM sample, the SO_4^{2-} doped samples present a characteristic peak around 1117 cm^{-1}, which is arisen from the asymmetric stretching modes of S—O unit belonging to sulfate

SO_4^{2-} group bending modes.[8,27] Meanwhile, no absorption from NH_4^+ group is observed. This result indicates that a small amount of SO_4^{2-} has been doped in the NCM particles.

In order to characterize the distribution of SO_4^{2-} in the cathode particles, the elemental composition on the cross section of a single spherical particle of NCMS-2 was analyzed using EDS. As shown in Figure 2a–e, Ni and Co are the dominant elements, while a small amount of Mn is enriched on the surface (≈ 1.5 μm), and S is dispersed on the cross section. The scattered S signals inside the section indicate that the sulfate is well incorporated into the NCM parent phase (Figure S5). The semi-quantitative EDS line scan analysis was carried out to NCMS-2 to obtain the profile of the element concentration (Figure 2f). For NCMS-2 (and other NCM samples), the Mn concentration decreases while the Ni and Co content increases complementarily from the surface to the center throughout the particle. The intensities of Ni, Co and Mn indicate that the CG structure of the cathode is obtained. EDS analysis demonstrates the non-uniform distribution of Mn in the particles, the CG distribution is inherited from the composite characteristics of pre-NCM. In this CG structure, the Ni-rich core provides high capacity, while the Mn-rich shell guarantees high cycle stability in the highly delithiated state. The intensity of S is stable from the center to the surface, indicating that the concentration of S is uniform. The sulfate doping may stabilize the bulk crystal structure and mitigate the undesired phase transformations. Such a distribution of dopants may simultaneously offer surface and bulk stability thus delivering favorable electrochemical properties.

Figure 3a,b shows the HRTEM images of NCMS-2 and corresponding fast Fourier transform (FFT) patterns (inset image in Figure 3b). The cathode particle exhibits two clear interplanar lattice fringes with the same distance of 0.239 nm at an angle of 120.8°. The two sets of the fringes correspond to the ($\bar{1}0\,0$) and ($\bar{1}\bar{1}0$) planes of NCM,[28,29] respectively. Meanwhile, the
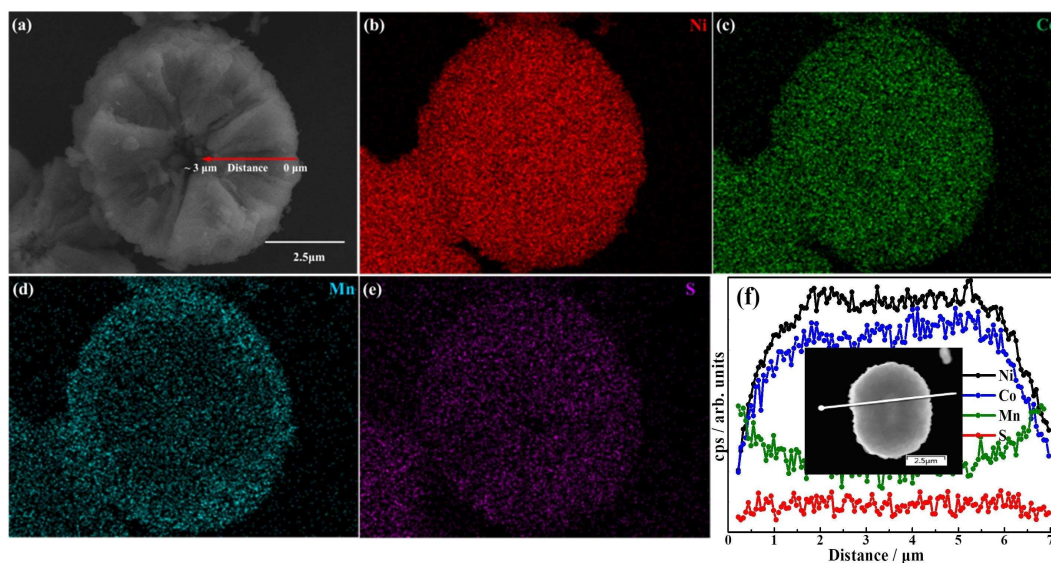

Figure 2. (a) SEM cross-sectional image of the NCMS-2 particle. (b–e) SEM EDS elemental mapping of NCMS-2 sample. (f) Corresponding element change trend of EDS line scan profile as a function of distance.
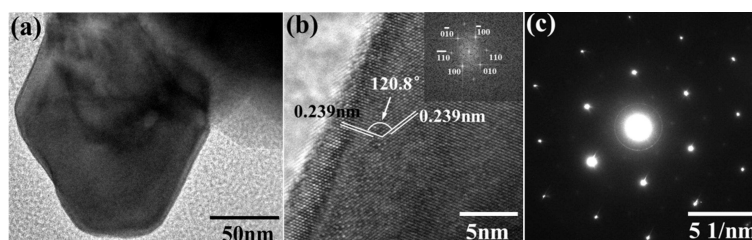
These are not the final page numbers! ↗↗

ChemSusChem

Full Papers
doi.org/10.1002/cssc.202100595

Chemistry
Europe
European Chemical
Societies Publishing

Figure 3. (a) TEM image, (b) HRTEM image (inset FFT), and (c) SAED pattern of NCMS-2.

selected area electron diffraction (SAED) along the [001] zone axis of the layered structure shown in Figure 3c confirms their layer structure.[30] These observations indicate that the cathode particles possess a well-defined layer structure with no impurity phases. The lattice parameters of the NCMS-4 particles showed in Figures S6 are the same as NCMS-2, indicating a same lattice structure for the two samples. Based on HRTEM observations, there is no direct evidence showing the presence of coating layer on the surface of the particles.

XANES spectra at Ni, Co, and Mn K-edges for three samples are shown in Figure 4, including the transition from the 1 s to unoccupied 3d orbital of the central TM ions (pre-edge peak marked by P) and the ligand-to-metal charge transfer from the 1 s to 4p orbital with and without shakedown process (marked by K and M, respectively).[31] The XANES spectra at Ni K-edges in Figure 4a show some changes in the shape of the edge (K) due to changes in the Ni local environment of a slightly distorted octahedral structure, and the peak of M shows a decrease in intensity and shifts to higher energies corresponding to oxidation after SO_4^{2-} doping.[32,33] The Co K-edge spectra in Figure 4b does not show a rigid shift toward higher energy but shows a decrease in intensity after SO_4^{2-} treatment. It is likely that the decreased intensity is due to the decreased coordination number caused by SO_4^{2-} doping in TM layers.[34,35] Changes are hardly observed in the Mn ion in Figure 4c, which indicates that SO_4^{2-} doping does not give rise to a distortion of Mn—O octahedron and Mn remains in the initial oxidation state. The trend of the variations for the bond length suggests that Ni—O
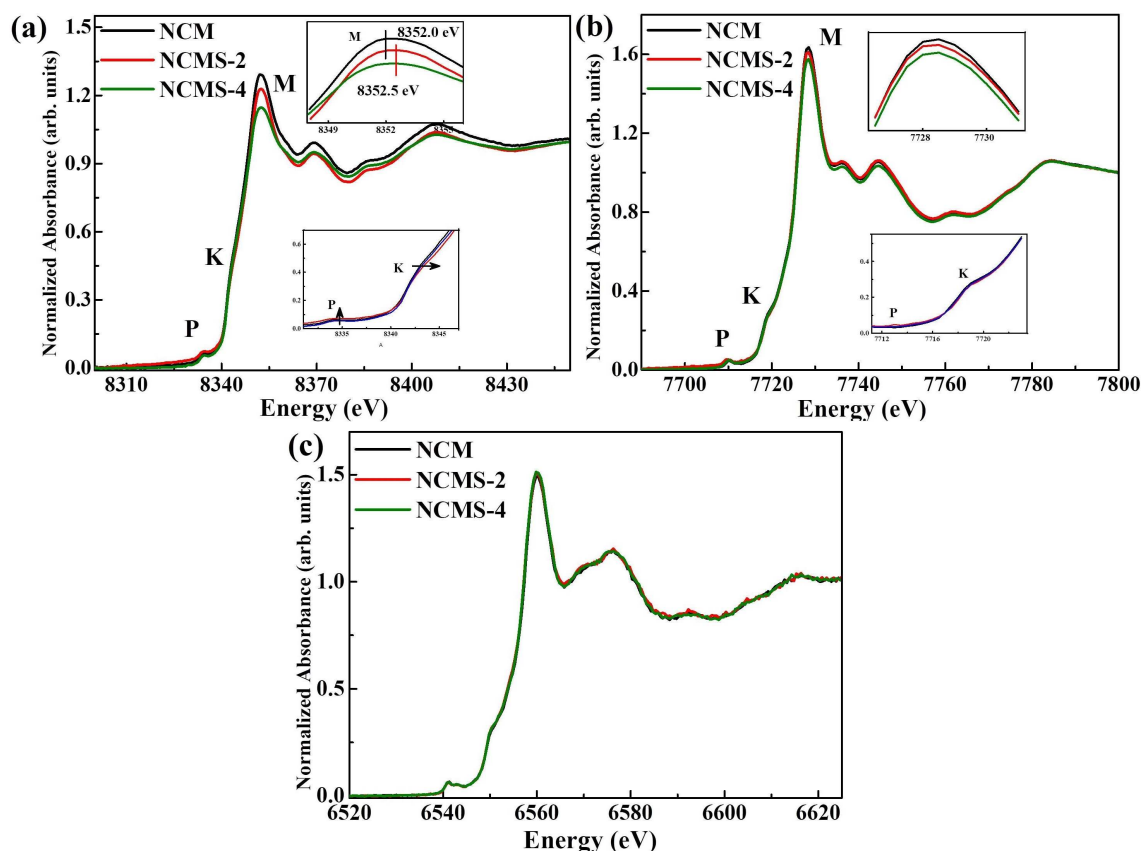

Figure 4. Normalized XANES spectra for NCM at (a) Ni, (b) Co, and (c) Mn.

These are not the final page numbers! ⬀⬀

ChemSusChem

Full Papers
doi.org/10.1002/cssc.202100595

Chemistry
Europe
European Chemical
Societies Publishing

and Co—O octahedron suffer from lattice distortion much more than Mn—O octahedron, which leads to a decrease in coordination number of Ni and Co (and a noticeable spectra intensity decrease). This may explain the observation that the Ni and Co are more vulnerable to structural distortion, as described in detail in the next DFT paragraph.

XPS technique was performed on three samples. The XPS full scan spectra of samples are given in Figure S7a. Binding energies of spectra were referenced to the C 1 s binding energy set at 284.8 eV (Figure S7b). The S 2p spectra of the samples (shown in Figure 5a) present two peaks at the binding energy of 170.2 and 169.1 eV, which can be assigned to S $2p_{3/2}$ and S $2p_{1/2}$ in the tetrahedral SO_4^{2-} groups.[27,36] In addition, the fitting curves of Ni 2p of the samples are plotted in Figure 5b. The oxidation state of Ni is a mixture of Ni^{2+} and Ni^{3+}, consistent with the previous reports.[37,38] NCMS has a higher Ni^{3+} content than NCM. The low Ni^{2+} content in NCMS is consistent with the low Ni/Li cation mixing degree in NCMS-2 from XRD result. The Co 2p curves in Figure 5c show a similar trend and the Co^{3+} content varies from 58.79 (NCM) to 60.08 and 60.41% (NCMS-2 and NCMS-4). This phenomenon can be explained by the charge compensation to balance the negatively charged SO_4^{2-}. At the same time, Mn is relatively stable after SO_4^{2-} doping, as shown in Figure 5d. Based on the above analysis, once SO_4^{2-} has been doped into the layer structure, the modified interaction between Ni (and Co) ions and Li would increase the average valence state, resulting in the decrease of cation mixing degree, which usually leads to a better electrochemical performance. This trend is also observed in PO_4^{3-} doped layer cathode and other anions-doped samples as previously reported.[25,39,40]

In order to investigate the effect of SO_4^{2-} on electrochemical performance of NCM, the initial charge/discharge profiles at 0.1 C between 2.8–4.3 V was studied as shown in Figure S8. All five samples present a stable and smooth voltage plateau in the initial charge/discharge (IC/IDC) process. This result indicates that the SO_4^{2-} doped in the layer structure causes no damage to the intrinsic electrochemical performance in the redox system. The IC/IDC capacities of the pristine NCM are 216.9/188.1 mAh g^{-1} and the corresponding columbic efficiency (CE) is 86.7%. With the increase of the SO_4^{2-} content in the NCM samples, the IC/IDC capacity and CE firstly increase and then decrease. The NCMS-2 sample exhibits the best performance, whose IC/IDC capacity is 220.2/196.9 mAh g^{-1} and CE is 89.4%. Further increase of SO_4^{2-} content, however, leads to poorer performance as shown in Table S4. The cycling performance of the pristine and SO_4^{2-} doped samples at 0.2 C are presented in Figure 6a. NCMS-2 exhibits the highest capacity retention of 80.9% after 380 cycles. Other samples suffer from obvious capacity fading as shown in table S5. Comparing the evolution of charge/discharge profiles of NCM and MCMS-2 from Figure 6b,c, it can be seen that voltage profiles of the NCMS-2 are basically identical, while the curve of NCM shifts sharply after 100 cycles. The voltage plateaus become indistinguishable,
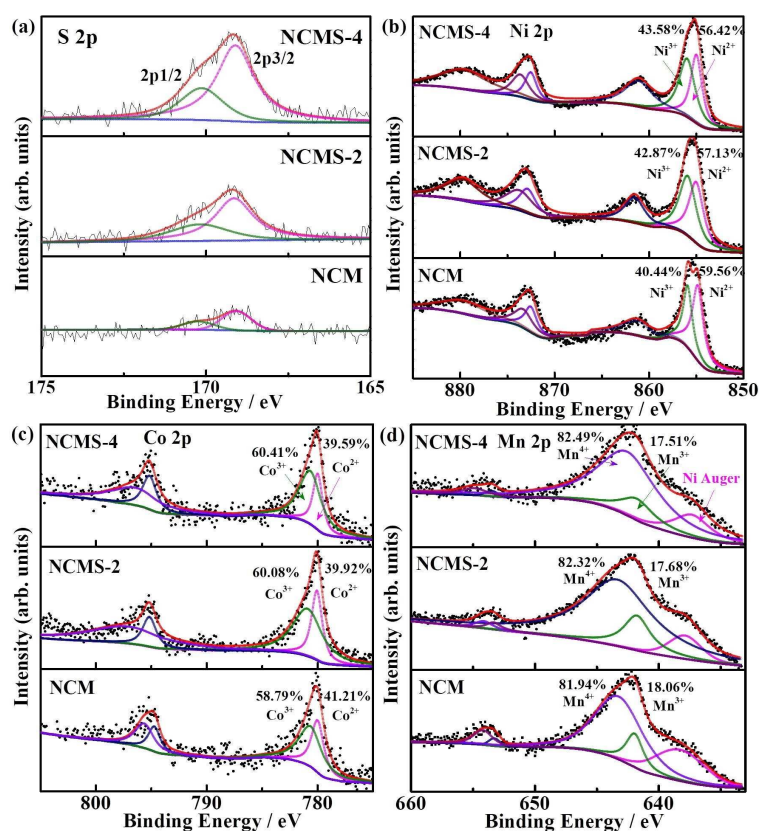

Figure 5. XPS spectra of (a) S 2p, (b) Ni 2p, (c) Co 2p, (d) Mn 2p core peaks for NCM materials doped with sulfate.
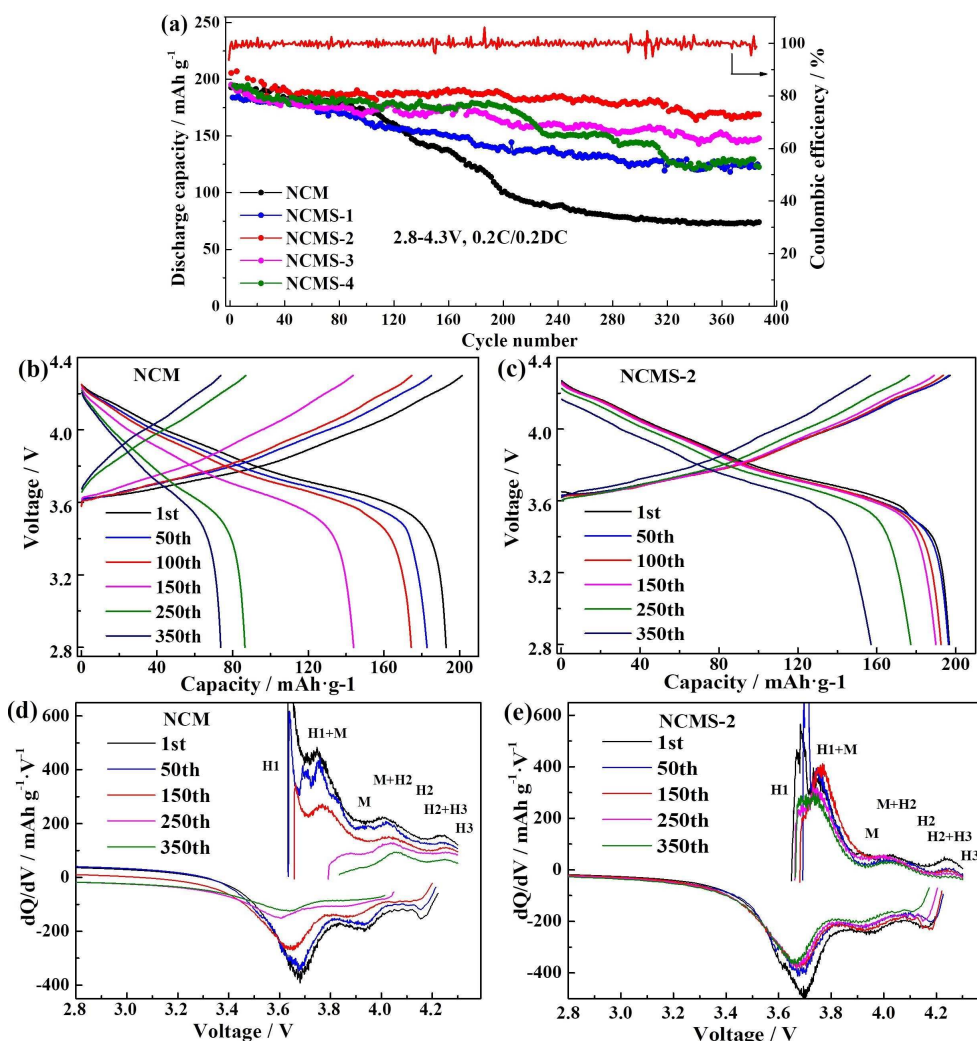
ChemSusChem

Full Papers
doi.org/10.1002/cssc.202100595

Chemistry Europe
European Chemical
Societies Publishing

Figure 6. (a) Cycling performance at 0.2 C of NCM materials. Charge/discharge profiles of selected cycles with (b) NCM and (c) NCMS-2. dQ/dV curves for (d) NCM and (e) NCMS-2 cathodes.

implying that NCM may suffer from serious irreversible structural changes upon cycling. The result indicates that appropriate amount of SO_4^{2-} doping can effectively improve the cycling stability. The improved cycling performance can be attributed to the atom-scale modification of SO_4^{2-}, which restrains the loss of active sites and makes the layered structure more stable in the cycling process.

To show structural changes in the cathodes during charge and discharge, differential capacity curve (dQ/dV) profiles were obtained by differentiating charge/discharge curves (Figure 6d,e). Considering the case of the NCM (Figure 6d), all three peaks experience decline in intensity after 380 cycles. The third peak (standing for the H3–H2 phase transition) suffers the most severe intensity reduction. Generally, the gradual decrease in the intensity of the H3–H2 redox peak with cycling is due to the reduction of the extent of H3 reversible transformation. H3–H2 phase transition would give rise to a strain, which may result in irreversible crystal structure transformation and even cause cracks in the electrode particles, and thus lead to an irreversible

structure transformation.[4] Compared with NCM, NCMS-2 has much smaller intensity decline, and the corresponding peaks (the area of these reactions) and voltage almost have no change. Accordingly, SO_4^{2-} plays an important role in stabilize the crystal structure of NCM during the electrochemical process by suppressing serious side reaction and maintaining the electrochemical active.

Figure S9a shows the rate performance of the pristine and SO_4^{2-} doped samples at various current densities between 2.8 and 4.3 V. The NCMS-2 shows the best rate performance, with discharge capacities of 193.7, 186.1, 178.0, 168.2, and 143.4 mAh g^{-1} at 0.2, 0.5, 1, 2, and 5 C, respectively. A discharge capacity of 195.4 mAh g^{-1} can be restored as the rate is changed back to 0.2 C rates. It can be seen that appropriate SO_4^{2-} doping in NCM brings about a better rate performance than the pristine and NCM samples with excessive SO_4^{2-} doping amount. The improvement also could be explained by the proper grain size as discussion in the XRD result. In order to evaluate the long-term stability of samples in high current, the

These are not the final page numbers! ↗↗

ChemSusChem

Full Papers
doi.org/10.1002/cssc.202100595

Chemistry Europe
European Chemical
Societies Publishing

cathodes are cycled at 1 C rate for 240 cycles, as shown in Figure S9b and Table S5. The capacity retention for NCMS-2 after 240 cycles is 80.4%, much higher than 28.6% for NCM. Coin cells using graphite as anode are cycled at 1 C rate for 250 cycles, as shown in Figure S9c and Table S5. The capacity retention for NCS-2 after 250 cycles is 85.9%. This excellent cycling stability of NCMS-2 demonstrates that SO_4^{2-} greatly improves the ability of the layer structure to endure larger current cycling.

After cycling, we examined the morphology of the particles by SEM (Figure S10). All the cathode samples give hazy appearance on the surface, particularly after 300 cycles. The primary crystalline grains become more loose, and the interstice between the crystalline grains become larger than the initial state after cycles. All indicate that the TM dissolution was occurred after cycles. TM dissolution could be deemed as one of the reason for the capacity decay of Ni-rich cathodes. ICP was also employed to look into the dissolution of TM in the cathode samples (Table S6). After 300 cycles, the atomic ratios of Ni, Co, and Mn elements of NCM reduce to 0.68:0.10:0.01, while that of NCMS-2 is 0.70:0.11:0.01. Despite the latter slightly higher TM content compared to the other samples, the difference of TM content in the five samples is still small. It seems that sulfate doping could suppress the capacity fading of Ni-rich cathodes but cannot restrain the dissolution of TM elements. Considering that a variety of degradations, such as cathode-electrolytes parasitic reactions, phase transformation, and surface reconstruction, could result in capacity fading,[41,42] sulfate doping might suppress the capacity fading from other aspects other than restraining TM dissolution in the Ni-rich cathode.

CV was executed to investigate the oxidation/reduction behavior of NCM materials. A linear relationship is observed between the peak current i_p and the square root of the scan rate ($v^{1/2}$), as shown in Figure S11c. The diffusion coefficient D_{Li^+} can be then estimated from the slope of the curve, which is calculated according to the Randles–Sevcik equation [Eq. (4)]:

$$i_p = 2.69 \times 10^5 n^{3/2} A D_{Li}^{1/2} v^{1/2} C_{Li} \tag{4}$$

where n represents the number of electrons per reaction species ($n \approx 1$ for NCM cathode), A is the surface area of the electrode, and C_{Li} refers to the bulk concentration of Li^+ in the electrode (given as 0.02378 mol cm^{-3}).[43] According to the slope of the fitted line, the estimated D_{Li^+} of the NCMS-2 and NCM samples are 1.73×10^{-14} and 5.03×10^{-15} cm^2 s^{-1}, respectively. The result suggests that the lithium-ion diffusion could be facilitated by the SO_4^{2-} doping, which is also in good agreement with the improved rate performance.

GITT was carried out to verify the role of SO_4^{2-} in kinetic properties improvement (Figure S12). It can be observed that the D_{Li^+} of NCMS-2 is approximately 3.13×10^{-15} cm^2 s^{-1} in the state of charge and 2.95×10^{-15} cm^2 s^{-1} in discharge process, which is higher than NCM ($\sim 2.62 \times 10^{-15}/\sim 2.31 \times 10^{-15}$ cm^2 s^{-1} in charge/discharge process). The results are consistent with the experimental measurements on CV experiment, which also manifests that SO_4^{2-} doping is beneficial to promoting the kinetic properties during cycles.

To investigate the changes of electrode resistance and reaction kinetics of the cathode materials, EIS was applied. Nyquist plots of NCM and NCMS electrodes in the charge state (≈ 4.1 V) in the 2nd, 100th, and 200th cycle are presented in Figure 7. In the equivalent circuit as shown in the inset of Figure 7a, R_s and R_{sf} represents the internal resistance and ion diffusion in the surface layer, and R_{ct} corresponds to interface charge transfer resistance at the electrode and electrolyte.[44,45] The relevant impendence values after different cycles are listed in Table S7. In the 2nd cycle, NCMS exhibit relatively smaller $R_s + R_{sf}$ and R_{ct} values compared with the NCM. Even after 200 cycles, the NCMS cathodes still maintain smaller resistance in the spectra. On the contrary, R_{ct} value of NCM reaches much higher after 200 cycles (in the inset of Figure 7b). These results suggest that SO_4^{2-} doping is beneficial to the interfacial stability, so as to indirectly preventing NCMS from subsequent side reactions.

To understand the structure stability of ployanions doping, we employed first-principles calculations with the CP2 K/Quickstep package to explore the occupancy site of SO_4^{2-} in NCM811 crystal. $Li_{48}SNi_{39}Co_4Mn_4O_{96}$ [$LiTM_{0.98}O_{1.92}(SO_4)_{0.02}$] is selected in
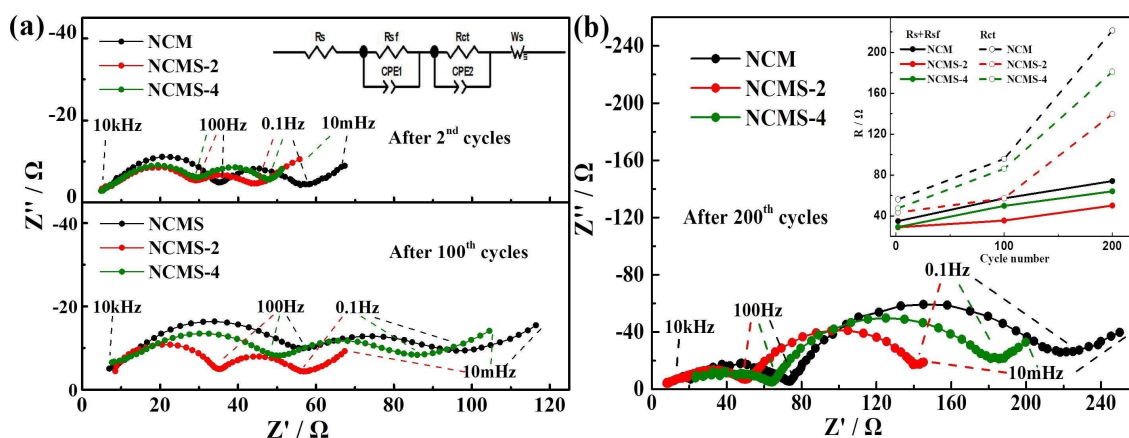

Figure 7. Nyquist plots of the NCM electrodes from 10 kHz to 10 mHz at approximately 4.2 V (a) after 2nd and 100th cycles and (b) after 200th cycle.

These are not the final page numbers! ↗↗

ChemSusChem

Full Papers
doi.org/10.1002/cssc.202100595

Chemistry Europe
European Chemical
Societies Publishing

our Ni-rich cathode. Three possible S spatial models are considered as shown in Figure S13a–c, where the S is separated by surrounding Co—O, Ni—O, and Mn—O octahedron, respectively. The calculated total energy for sulfate doped at different sites in the system is shown in Figure S13d. Lower energy values generally represent thermodynamically favorable system. As can be seen from curves, the doping of S atom surrounded by Ni—O possesses the lowest energy, revealing that doping of S in the system of Ni—O—S is feasible. When the Ni ions are replaced with sulfate, the local coulombic interaction of the related TM ions is changed, and the network of coulombic interactions among the TM ions (including the TM—O octahedral) is also broken. This relation can help us to better understand the role of each individual TM ions in NCM. The Ni—O—S structure has the lowest energy, suggesting that Ni is the weakest bond in the layer structure. Although a bit more strongly bound, the behavior of Co ions is relatively similar to Ni, giving rise to slight destruction of symmetry. On the other hand, Mn strongly stabilizes the layered structure, as the dopant substitution causes the highest energy arrangement. These results are consistent with the experimental evidence that the role of Mn is mainly to improve the phase stability of layered oxides.[46] In summary, the structure models using the DFT methods show trends comparable to the XANES and XPS experimental. Sulfate doping induces the symmetry-broken of NiO_6 octahedral (and followed by CoO_6), and thereby influences the oxidation state and electronic properties of the material significantly.

Since the S atom surrounded by Ni—O system has the lowest energy among all sites, the Ni—O—S structure was hence chosen for further calculations. Thus, the coulombic interaction caused by sulfate doping will give rise to the distortion and lead to the improved diffusion coefficient in the bulk structure. To better understand the process, energy barriers for Li-ion migration in Ni—O—S model were calculated. In the natural layer structure, as shown in Figure 8, the energy barrier for Li migration along the Co—O intermediate and Mn—O intermediate is 0.50 and 0.49 eV, respectively. The results are comparable to the values of Li migration (0.36–0.52 eV) reported previously.[47,48] However, in the SO_4^{2-} doping case, the energy barrier value is only 0.17 eV. It indicates that Li ions would migrate much easier when Ni—O

is broken caused by SO_4^{2-} doping. In brief, the symmetry breaking of Ni—O octahedral resulting from sulfate doping surrounded by Ni—O determines the diffusion pathway featuring structure and electrochemical stabilization.

Conclusion

SO_4^{2-} impurity has been widely accepted as a deficiency in layer Li[$Ni_{0.8}Co_{0.15}Mn_{0.05}$]$O_2$ (NCM) cathodes, but this comprehensive study on the role played by sulfate in NCM cathode shows that a proper amount of sulfate (0.6 wt% in NCM) has a beneficial effect on the performance. The enhanced properties can be attributed to the proper grain size and the embedding of polyanions SO_4^{2-} into the layer structure of NCM. Electrochemical characterizations certify that a proper sulfate doping in NCM could improve the rate performance and the cycling performance. X-ray absorption near edge structure and X-ray photoelectron spectroscopy experiments results and the density functional theory calculation indicate that the dopant is inclined to be surrounded by Ni—O, followed by Co—O octahedral. The doped site of sulfate in transition metal layer plays a crucial role in governing the Li-ion diffusion. Through first-principles calculations, very low activation energy (0.17 eV) for Li$^+$ migration is observed, and this declined activation energy can be attributed to the symmetry distortion of NiO_6 octahedral. In summary, SO_4^{2-} doping affects the local coulombic interaction, which leads to lattice distortion of Ni—O octahedral, reduces the Li$^+$ migration energy, and suppresses the *c* axis contraction during cycling. The phase transition of H2–H3 and mechanical strain caused by the *c* axis contraction are hence suppressed and the cycling performance is enhanced. These experiments indicate that the strict standards for sulfate content in pre-NCM for cathode materials may be relaxed, which could cut down the water consumption and reduce the cost of cathode NCM manufacturing without causing a decrease in cell performance. The subsequent work in large-quantity synthesis of NCM in pouch cell is the next frontier.

Conflict of Interest
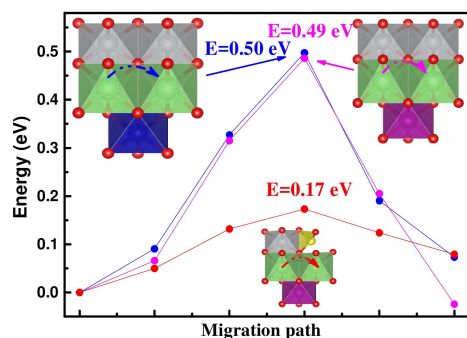
The authors declare no conflict of interest.

Figure 8. Li migration paths between neighboring octahedral sites via an intermediate Co—O and Mn—O octahedral site, and the corresponding migration barriers.

[1] P. Yan, J. Zheng, J. Liu, B. Wang, X. Cheng, Y. Zhang, X. Sun, C. Wang, J. G. Zhang, *Nat. Energy* **2018**, *3*, 600–605.
[2] J. B. Goodenough, K. S. Park, *J. Am. Chem. Soc.* **2013**, *135*, 1167–1176.

ChemSusChem

Full Papers
doi.org/10.1002/cssc.202100595

Chemistry Europe
European Chemical
Societies Publishing

[3] J. L. Shi, D. D. Xiao, M. Ge, X. Yu, Y. Chu, X. Huang, X. D. Zhang, Y. X. Yin, X. Q. Yang, Y. G. Guo, L. Gu, L. J. Wan, *Adv. Mater.* **2018**, *30*, 1705575–1705583.

[4] U.-H. Kim, L.-Y. Kuo, P. Kaghazchi, C. S. Yoon, Y.-K. Sun, *ACS Energy Lett.* **2019**, *4*, 576–582.

[5] C. S. Yoon, K. J. Park, U. H. Kim, K. H. Kang, H. H. Ryu, Y. K. Sun, *Chem. Mater.* **2017**, *29*, 10436–10445.

[6] T. He, Y. Lu, Y. Su, L. Bao, J. Tan, L. Chen, Q. Zhang, W. Li, S. Chen, F. Wu, *ChemSusChem* **2014**, *11*, 1639.

[7] Q. Ni, Y. Bai, F. Wu, C. Wu, *Adv. Sci.* **2017**, *4*, 1600275–1600298.

[8] L. Ban, Y. Yin, W. Zhuang, H. Lu, Z. Wang, S. Lu, *Electrochim. Acta* **2015**, *180*, 218–226.

[9] C. H. Jo, D. H. Cho, H. J. Noh, H. Yashiro, Y. K. Sun, S. T. Myung, *Nano Res.* **2014**, *8*, 1464–1479.

[10] K. Min, K. Park, S. Y. Park, S.-W. Seo, B. Choi, E. Cho, *J. Electrochem. Soc.* **2018**, *165*, 79–85.

[11] J. VandeVondele, M. Krack, F. Mohamed, M. Parrinello, T. Chassaing, J. Hutter, *Comput. Phys. Commun.* **2005**, *167*, 103–128.

[12] S. Goedecker, M. Teter, J. Hutter, *Phys. Rev. B* **1996**, *54*, 1703–1710.

[13] J. VandeVondele, J. Hutter, *J. Chem. Phys.* **2007**, *127*, 114105–114108.

[14] J. P. Perdew, K. Burke, M. Ernzerhof, *Phys. Rev. Lett.* **1996**, *77*, 3865–3868.

[15] G. Henkelman, B. P. Uberuaga, H. Jónsson, *J. Chem. Phys.* **2000**, *113*, 9901–9904.

[16] K. Momma, F. Izumi, *J. Appl. Crystallogr.* **2011**, *44*, 1272–1276.

[17] Y. J. Shi, H. Shu, Y. H. Zhang, H. M. Fan, Y. P. Zhang, L. J. Yang, *Fuel Process. Technol.* **2016**, *150*, 141–147.

[18] W. D. Halstead, *J. Appl. Chem.* **1970**, *20*, 129–132.

[19] B.-B. Lim, S.-T. Myung, C. S. Yoon, Y.-K. Sun, *ACS Energy Lett.* **2016**, *1*, 283–289.

[20] J. M. Wikberg, M. Dahbi, I. Saadoune, T. Gustafsson, K. Edström, P. Svedlindh, *J. Appl. Phys.* **2010**, *108*, 083909–083913.

[21] C. S. Yoon, D.-W. Jun, S.-T. Myung, Y.-K. Sun, *ACS Energy Lett.* **2017**, *2*, 1150–1155.

[22] C. Abram, J. Shan, X. Yang, C. Yan, D. Steingart, Y. Ju, *ACS Appl. Mater. Interfaces* **2019**, *2*, 1319–1329.

[23] W. Li, X. Liu, H. Celio, P. Smith, A. Dolocan, M. Chi, A. Manthiram, *Adv. Energy Mater.* **2018**, 1703154–1703164.

[24] L. Azhari, X. Zhou, B. Sousa, Z. Yang, G. Gao, Y. Wang, *ACS Appl. Mater. Interfaces* **2020**, *12*, 57963–57974.

[25] Y. Zhao, J. Liu, S. Wang, R. Ji, Q. Xia, Z. Ding, W. Wei, Y. Liu, P. Wang, D. G. Ivey, *Adv. Funct. Mater.* **2016**, *26*, 4760–4767.

[26] H. Z. Zhang, F. Li, G. L. Pan, G. R. Li, X. P. Gao, *J. Electrochem. Soc.* **2015**, *162*, A1899–A1904.

[27] D. Ye, R. Qu, H. Song, X. Gao, Z. Luo, M. Ni, K. Cen, *Chem. Eng. J.* **2016**, *283*, 846–854.

[28] F. Fu, G. L. Xu, Q. Wang, Y. P. Deng, X. Li, J. T. Li, L. Huang, S. G. Sun, *J. Mater. Chem. A.* **2013**, *1*, 3860–3864.

[29] W. Pi, T. Mei, Z. Zhang, X. Li, J. Wang, J. Li, X. Wang, *CrystEngComm* **2017**, *19*, 442–446.

[30] W. Hua, J. Zhang, Z. Zheng, W. Liu, X. Peng, X. D. Guo, B. Zhong, Y. J. Wang, X. Wang, *Dalton Trans.* **2014**, *43*, 14824–14832.

[31] D. Ahn, I. Yoo, Y. Koo, N. Shin, J. Kim, T. J. Shin, *J. Mater. Chem.* **2011**, *21*, 5282–5289.

[32] S. H. Kim, C. S. Kim, *J. Electroceram.* **2008**, *23*, 254–257.

[33] W. S. Yoon, M. Balasubramanian, K. Y. Chung, X. Q. Yang, J. McBreen, C. P. Grey, D. A. Fischer, *J. Am. Chem. Soc.* **2005**, *127*, 17479–17487.

[34] E. M. Erickson, H. Sclar, F. Schipper, J. Liu, R. Tian, C. Ghanty, L. Burstein, N. Leifer, J. Grinblat, M. Talianker, J. Y. Shin, J. K. Lampert, B. Markovsky, A. I. Frenkel, D. Aurbach, *Adv. Energy Mater.* **2017**, *7*, 1700708–1700717.

[35] M. J. Zhang, G. Teng, Y. K. Chen-Wiegart, Y. Duan, J. Y. P. Ko, J. Zheng, J. Thieme, E. Dooryhee, Z. Chen, J. Bai, K. Amine, F. Pan, F. Wang, *J. Am. Chem. Soc.* **2018**, *140*, 12484–12492.

[36] A. Q. Turin, G. Vallverdu, D. Flahaut, J. Allouche, L. Croguennec, M. Menetrier, I. Baraille, *ACS Appl. Mater. Interfaces* **2017**, *9*, 44922–44930.

[37] S. Xia, F. Li, F. Cheng, X. Li, C. Sun, J. J. Liu, H. Guo, *J. Electrochem. Soc.* **2018**, *165*, A1019–A1026.

[38] G. Hu, Z. Zhang, T. Li, Z. Gan, K. Du, Z. Peng, J. Xia, Y. Tao, Y. Cao, *ChemSusChem* **2019**, *13*, 1603–1612.

[39] K. Liu, Q. Zhang, S. Dai, W. Li, X. Liu, F. Ding, J. Zhang, *ACS Appl. Mater. Interfaces* **2018**, *10*, 34153–34162.

[40] L. Qiu, W. Xiang, W. Tian, C. Xu, Y. Li, Z. Wu, T. Chen, K. Jia, D. Wang, F. He, X. Guo, *Nano Energy* **2019**, *63*, 103818–103826.

[41] H. M. K. Sari, X. Li, *Adv. Energy Mater.* **2019**, *9*, 1901597–1901627.

[42] G. Xu, X. Liu, A. Daali, R. Amine, Z. Chen, K. Amine, *Adv. Funct. Mater.* **2020**, *30*, 2004748–2004792.

[43] C. Yin, H. Zhou, Z. Yang, J. Li, *ACS Appl. Mater. Interfaces* **2018**, *10*, 13625–13634.

[44] W. Liu, Q. Shi, Q. Qu, T. Gao, G. Zhu, J. Shao, H. Zheng, *J. Mater. Chem. A* **2017**, *5*, 145–154.

[45] W. Liu, X. F. Li, D. B. Xiong, Y. C. Hao, J. W. Li, H. R. Kou, B. Yan, D. J. Li, S. G. Lu, A. Koo, K. Adair, X. L. Sun, *Nano Energy* **2018**, *44*, 111–120.

[46] C. Liang, F. Kong, R. C. Longo, C. Zhang, Y. Nie, Y. Zheng, K. Cho, *J. Mater. Chem. A* **2017**, *5*, 25303–25313.

[47] K. Kang, Y. S. Meng, J. Breger, C. P. Grey, G. Ceder, *Science* **2006**, *311*, 977–980.

[48] Y. Wei, J. Zheng, S. Cui, X. Song, Y. Su, W. Deng, Z. Wu, X. Wang, W. Wang, M. Rao, Y. Lin, C. Wang, K. Amine, F. Pan, *J. Am. Chem. Soc.* **2015**, *137*, 8364–8367.

FULL PAPERS

How much sulfate? 0.6 wt% SO_4^{2-} doping affects the local coulombic interaction, which leads to lattice distortion of Ni—O octahedral, and the energy barrier for Li^+ migration along the Ni—O intermediate is only 0.17 eV. The phase transition of H2 to H3 and mechanical strain caused by the *c* axis contraction can hence be suppressed during cycling and the cycling performance is enhanced.
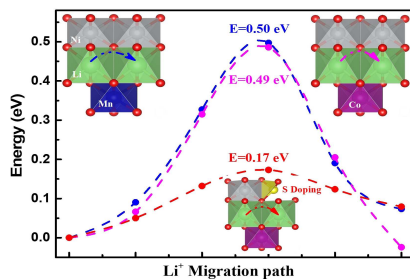
J. Li, J. Wu, S. Li, Dr. G. Liu, Prof. Y. Cui, Prof. Z. Dong*, Prof. H. Liu*, X. Sun

1 – 11

Stabilizing LiNi$_{0.8}$Co$_{0.15}$Mn$_{0.05}$O$_2$ Cathode by Doping Sulfate for Lithium-Ion Batteries